J. Mech. Phys. Solids 170 (2023) 105094

Contents lists available at ScienceDirect

Journal of the Mechanics and Physics of Solids

journal homepage: www.elsevier.com/locate/jmps

Scaling in size, time and risk—The problem of huge extrapolations and remedy by asymptotic matching

Zdeněk P. Bažant [a,*,1], Hoang T. Nguyen [b], A. Abdullah Dönmez [c,2]

[a] Northwestern University, 2145 Sheridan Road, CEE/A135, Evanston, IL 60208, United States of America
[b] Brown University, United States of America
[c] Northwestern University, United States of America

ARTICLE INFO

In honor of Professor Yonggang Huang at the occasion of his 60th birthday

Keywords:
Fracture mechanics
Size effect on strength
Creep and shrinkage
Water diffusion
Cement hydration
Failure probability
Experimental databases
Concrete structures

ABSTRACT

The scaling of structural response of concrete structures to large structure sizes, to long service lives and to tolerable failure probabilities is a problem of order-of-magnitude extrapolations, which are intractable by AI and machine learning and require significant theoretical advances. The present review, based on a lecture at Yonggang Huang's 60th birthday symposium in Houston, summarizes the recent advances, with a focus on those achieved at Northwestern University. Reliable extrapolation requires two-sided asymptotic matching. Most existing databases provide support on only one extreme of the range of size, time or failure probability, but theoretical support can be obtained for the asymptotic behaviors on both sides of the range. The advantage is that the asymptotics are much simpler than the behavior in the central, transitional, range. In closing it is explained that realistic extrapolations are required to mitigate the calamitous CO_2 emissions from cement and concrete industry.

1. Problem faced

While artificial intelligence, with machine learning and deep learning, has recently gained enormous popularity and enabled the tackling of some difficult problems, the problems requiring major, orders-of-magnitude, extrapolations from the existing database are beyond its reach. For such problems, a physics based mathematical theory, with at least indirect experimental verification, is indispensable.

Among all the fields of engineering, structural engineering is special in that it requires enormous extrapolations. Thousands of bridges, buildings, and other large structures, each different, must be designed without being able to test full scale prototypes. This necessitates order-of-magnitude extrapolation from the lab to the structure size. In addition, century-plus durability, several orders of magnitude beyond the time span of experiments, is demanded. On top of that, the tolerable probability of failure, or risk, is about four orders of magnitude below the feasible range of testing, and even of quantifiable experience.

One consequence of these predicaments is that the concrete design code, such as ACI Standard 318, requires safety margins that are in some situations enormous and in others wasteful. Yet the safety record is imperfect, as numerous spectacular failures and drastically shortened lifetimes document. Unlike aeronautical, automotive, electronic, and other engineering, structural engineering cannot exist without a detailed design code because many thousands of structures, each different, with hundreds of different concrete

* Corresponding author.
E-mail address: z-bazant@northwestern.edu (Z.P. Bažant).
[1] McCormick Institute Professor and W.P. Murphy Professor of Civil and Mechanical Engineering and Materials Science.
[2] On leave from Istanbul Technical University.

https://doi.org/10.1016/j.jmps.2022.105094
Received 11 September 2022; Accepted 2 October 2022
Available online 17 October 2022
0022-5096/

compositions undefined a priori, must be designed. Large databases of laboratory experimental data for many different concretes have been assembled from worldwide literature, but they suffer from three kinds of bias (Fig. 1a):

(a) **Size:** In the worldwide database of laboratory tests of the shear strength of reinforced concrete (RC) (initially assembled at Northwestern (Bažant and Kim, 1984) and expanded by ACI-445F to about 800 tests), 81% of data concern cross-sections smaller than 0.4 m and 98% smaller than 1.25 m while girders of cross-section size up to 15 m are being built.

(b) **Time:** For creep and shrinkage, whose correct prediction helps to suppress distributed cracking, which is crucial for durability, 95% of the 4000^+ test curves assembled worldwide are limited to a 6-year duration, 99% to a 12-year duration, and two tests to a 30-year duration, while bridges are supposed to last well over a century.

(c) **Risk:** This is the problem of failure probability, P_f, underpinning the "understrength" safety factors as well as the big, yet hidden, safety margins built into the supposedly deterministic equations of the design code. As safety experts generally agree, the P_f per lifetime of bridges, aircraft, and computer chips, should not exceed one in a million (or 10^{-6}) per lifetime. This is the probability of being killed for example by a falling tree, lightning, or wild animal. However, the existing evidence suffices to verify failure probabilities no lower than one in thirty, or $3 \cdot 10^{-2}$. So, an extrapolation by 4 orders of magnitude is necessary. The only way to tackle it is by linking it to the theory of size effect.

The gist of this review article is to emphasize that the extrapolations can be facilitated by exploiting the asymptotic properties, which are deduced from physics and are often relatively simple. Using only one-sided asymptotic properties would not avoid the inevitable errors of extrapolation. So, what is proposed here, is to exploit asymptotic properties at the opposite ends of the range, i.e., pursue two-sided asymptotic matching even if the experimental basis exists only on one side.

It is unfortunate but inevitable that the experimental databases exist only for small sizes, short times, and medium probabilities. But the physical asymptotic properties can be theoretically derived for both sides—small and large sizes, short and long times, medium and extra-small probabilities. They suffice for great improvement of prediction. The point is to find out how to match them.

The review that follows is based mostly on the results obtained at Northwestern University. They are, of course, underpinned by extensive background literature (Alfredo and Tang, 1984; Askarinejad and Rahbar, 2015; Barenblatt, 1979, 2003; Charles, 1958; Chen et al., 2007; Coleman, 1958; Cusatis and Schauffert, 2009; Di Luzio and Cusatis, 2018; Daniels, 1945; Duckett, 2005; Dutta et al., 2013; Dutta and Tekalur, 2014; Evans, 1972; Evans and Fu, 1984; Fett, 1992; Fett and Munz, 1990; Fisher and Tippett, 1928; Jayatilaka and Trustrum, 1977; Gao et al., 2003; Glasstone et al., 1941; Griffith, 1921; Gumbel, 2004; Haldar and Mahadevan, 2000; Harlow and Phoenix, 1979, 1978; Harlow et al., 1983; Irwin, 1958; Krausz, 1988; Kramers, 1940; Le, 2015; Le et al., 2015, 2014; Melchers and Beck, 2018; Munz and Fett, 1999; Phoenix, 1978b; Phoenix et al., 1997; Rice et al., 1968; Shao et al., 2012; Wang et al., 2001; Wei et al., 2015; Weibull, 1939; Xu and Le, 2018; Zhurkov and Korsukov, 1974; Bažant and Le, 2009; Bažant et al., 2009; Coleman, 1957; Graham-Brady et al., 2006; Ibnabdeljalil and Phoenix, 1995; Lohbauer et al., 2002; Mahesh and Phoenix, 2004; Phillips and Rob, 2001; Phoenix, 1978a; Phoenix and Tierney, 1983; Smith, 1982; Thouless et al., 1983; Tobolsky and Eyring, 1943; Wagner, 1989; ACI318, 2019; Okamura and Higai, 1980; Iguro et al., 1984), but its discussion is beyond the scope of this article.

2. Size

The size effect has been the main or partial cause of a host of major failures (Fig. 1b). The fundamental problem is that of scaling when geometrically similar systems or structures of different sizes are compared. Here the fundamental concept is that of self-similarity (Barenblatt, 1979, 2003; Bažant and Oh, 1983). Let function $f(D, D_0)$ give the response (such as structure strength) at size D if D_0 is taken as the reference size. A process is self-similar if any other size D_1 can be taken as a reference size giving a similar response. This condition leads to the functional equation (Bažant et al., 2021; Bažant, 2002; Bažant and Le, 2017; Bažant and Planas, 2019):

$$\frac{f(D/D_0)}{f(D_1/D_0)} = f(D/D_1) \tag{1}$$

It can be verified that its solution is a power law $\sigma_N \propto D^n$ of any exponent n ($\sigma_N = P/A$ = nominal structure strength, A = characteristic cross-section area). Fig. 1c shows in a log–log plot the opposite asymptotes for the case of quasibrittle materials, representing power laws of exponents 0 and $-1/2$ (Fig. 1c). The horizontal asymptote is determined by the material strength, f_t, and the inclined one by the material fracture energy G_f.

2.1. Size effect of Type 2

In quasibrittle materials, the transition between these two asymptotes is best determined energetically. For this purpose we consider geometrically similar specimens of different sizes, with geometrically similar cracks or notches. We also assume that not only the man-made notches but also the critical cracks at maximum loads in structures of different size are geometrically similar. This is a frequent situation, especially for reinforced concrete. It is called the Type 2 failure, which occurs when an initially negative structure geometry changes to positive (i.e., when $[\partial K_I/\partial a]_P$ flips sign from negative to positive; K_I = stress intensity factor, a = crack length, P = load).

The energy released by unloading of the band that is traced by the advancing fracture process zone (FPZ) of finite width, w_0, is proportional to the crack band length, a, while the energy released from the rest of the structure is proportional to a^2 (Fig. 1d). The

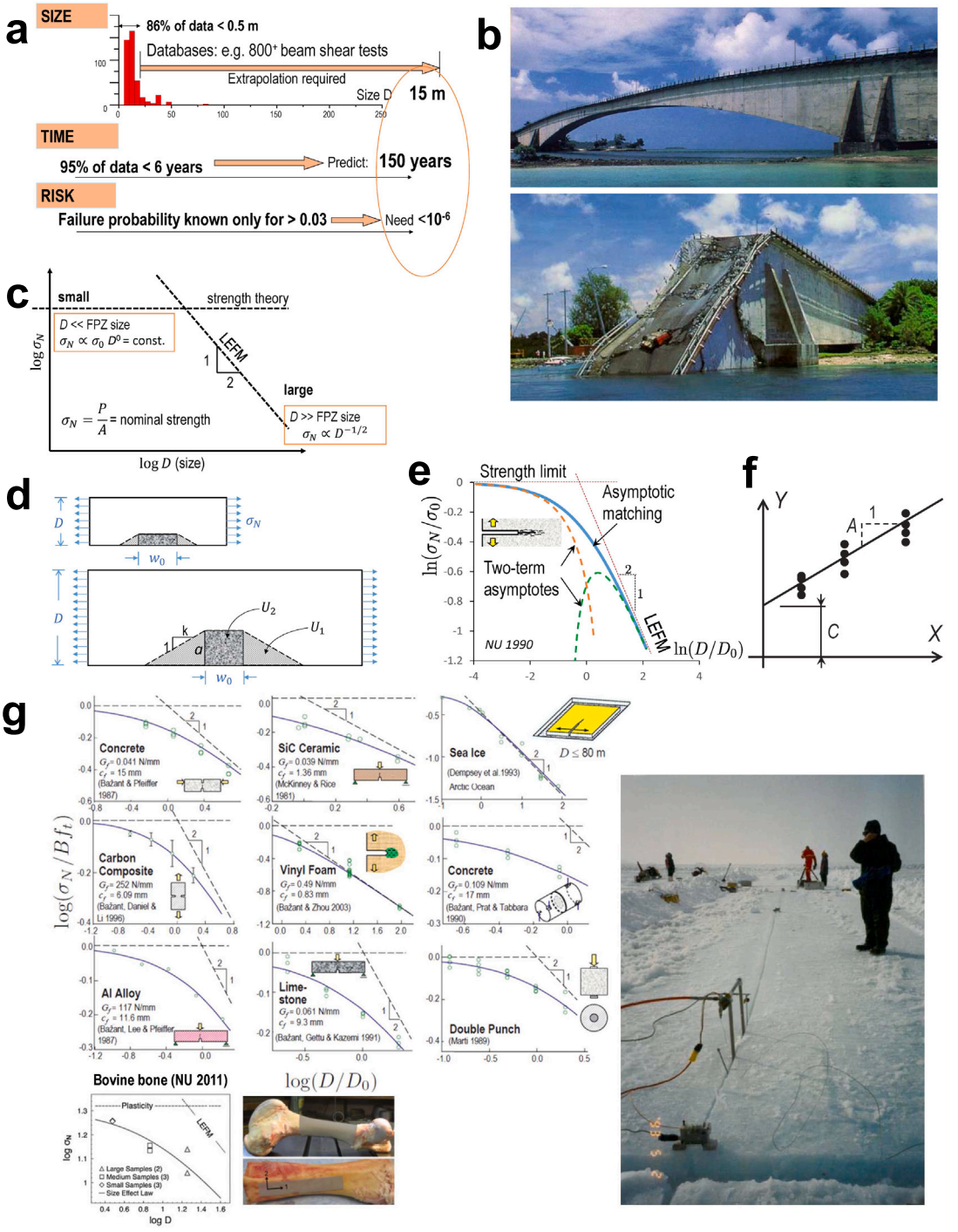

Fig. 1. (a) Three kinds of bias of the databases, (b) the collapse of KB Bridge in Palau, (c) two-asymptotes of the size effect law, (d) geometrical scaling of structures, (e) asymptotic matching with the SEL, (f) linear regression of the SEL, (g) size effect trend of different materials, with a photo of 24 m long notch, crack mouth gauge and flat jack pipes in floating sea ice plate 80 × 80 × 1.79 m in size, tested by John Dempsey et al. (in collaboration with Z.P. Bažant) in 1993.

condition of energy balance and the assumption that a/D = constant then yield the energetic size effect law (SEL) (Bažant, 1984)

of the form:

$$\sigma_N = N f_t' = B\sigma_0 \left(1 + \frac{D}{D_0}\right)^{-1/2} \tag{2}$$

where σ_0 material strength, B = constant dependent on structure and crack geometry. The opposite asymptotes of this formula are the power laws shown by the straight lines Fig. 1c. Note that the energetic derivation excludes other formulas that have the same straight-line asymptotes, such as $\sigma_N \propto 1/(1+\sqrt{D/D_0})$. Also note that the transition from one asymptote to the other is spread over three orders of magnitude and is the most important aspect of scaling (this aspect is not present in the renormalization group theory of quantum mechanics in which self-similarity and power laws have played since the 1950s a major role, but in a different way).

A more robust support for the size effect law can be obtained from the second-order asymptotic approximations obtained by the asymptotic expansions of: (1) the cohesive crack model for $D \to 0$ (this model closely approximates the crack band model in absence of crack-parallel stress), and (2) the linear elastic fracture mechanics (LEFM) for $D \to \infty$. This yields the first- and second-order terms of the asymptotic expansions:

$$\text{for } D \to 0: \quad \sigma_N \propto \sigma_0 - c_0 D + \cdots \tag{3}$$

$$\text{for } D \to \infty: \quad \sigma_N \propto D^{-1/2}(b_1 - b_2 D^{-1} + \cdots) \tag{4}$$

where σ_0, c_0, b_1, b_2 are constants. For $D \to 0$, the two-term asymptotic approximation is better obtained by the perturbation method in which the displacements, strains, and stresses are each expanded into a series of powers D^p where p is a constant, i.e.,

$$\text{for } D \to 0: \quad u_i = u_i^0 + u_i^1 D^{-p}, \ldots \quad \sigma_N = \sigma_N^0 + \sigma_N^1 D^{-p} + \cdots \tag{5}$$

If the terms with the same powers of D are isolated in the differential equations, cohesive crack law and boundary conditions, one gets a series of elasticity problems. The first two of them show that σ_N for $D \to 0$ must be approached linearly in D (which looks in the $\log D$-scale like an exponential approach).

The two-term asymptotic approximations are plotted in Fig. 1e by the dashed curves. It can be checked that the solid curve, representing the size effect law, represents the two-sided two-term (second-order) asymptotic matching of the foregoing two-term asymptotic approximations.

The asymptotic approximation of LEFM for $D \to \infty$ based on the assumption of constant fracture process zone length, as presented in 1990 in Bažant et al. (1990), express the first two large-size terms by means of the dimensionless energy release function $g(\alpha)$. This function depends only on the structure and crack geometry ($\alpha = a/D$ = relative length of the crack or notch, a = its actual length). This reveals that the SEL can be expressed in terms of the LEFM functions:

$$\sigma_N = \sqrt{\frac{E' G_f}{g'(\alpha_0) c_f + g(\alpha_0) D}} \tag{6}$$

where α_0 = relative length of a notch or initial stress-free crack, $E' = E$ = Young's modulus for plane stress and $E/(1-\nu^2)$ for plane strain ν = Poisson ratio, and c_f = material characteristic length (which for concrete equals about 30% to 40% of Irwin's length).

Eq. (6) has the advantage that it can be rearranged into a linear regression plot (Fig. 1f)

$$Y = AX + C \tag{7}$$

$$\text{where } X = D, \quad Y = \frac{E'}{g'(\alpha_0)\sigma_N^2} \tag{8}$$

After determining A and C by linear regression of the strength data for specimens of various sizes (Fig. 1e), one can calculate c_f and the fracture energy, G_f, of the material. This method became in 1989 the international standard recommendation of RILEM (Bažant, 1990; Bažant and Kazemi, 1991) for the testing of fracture energy of concrete and geomaterials, and was later also endorsed by the committee ACI-446.

The SEL has been shown to fit well the size effect data for notched fracture test specimens of all kinds of quasibrittle materials (see Fig. 1g), including, besides concrete, sea ice, tough ceramics, fiber composites, stiff foams, rock, wood, bone, etc. The biggest tests were those of floating compact tension specimens of first-year sea ice 1.79 m thick, geometrically scaled up from size 0.5×0.5 m to reach the size of 80 × 80 m (photo in Fig. 1g). They were loaded by a flat jack inserted into the notches, which ranged up to 24 m in length (the tests, organized and directed by John Dempsey from Clarkson University in collaboration with Bažant, were conducted West of Cornwallis Island, about 500 km North of Canadian mainland). These tests dispelled the previous belief that fracture mechanics did not apply to sea ice. They revealed that the effective FPZ size of sea ice for the horizontal growth of through-thickness cracks is several meters in length, and that the LEFM for horizontal fracture growth applies only at sizes > 20 m. This, for example, clarified why the forces measured on the legs of oil platforms, exerted by moving sea ice, are order-of-magnitude less than predicted by computer programs based on plasticity and buckling.

2.2. Size effects laws applicable when various mechanisms interfere

Due to interactions of various failure mechanisms, other asymptotic power laws have been obtained for the scaling of the strength of some other structural systems. Axially compressed unidirectional carbon-polymer composites fail by a kink band in which the strength is controlled by shear slip between axial splitting cracks, with axial buckling, which has traditionally been treated by

plasticity. This classical approach, which is adequate only when extrapolations to larger sizes are not of interest, has led to simple formulas of Rosen (1964), improved by Budiansky and Fleck (1993). However, scaled size effect tests of fiber-reinforced PEEK (polyether-ether-ketone) at Northwestern in 1999 (Bažant et al., 1999) demonstrated that the failure is not simultaneous, as required by plasticity. Rather, the compressed kink band propagates laterally, which is governed by fracture mechanics (i.e., by energy release rate) and leads to a generalized scaling law with constant residual strength σ^R (Bažant, 2002):

$$\sigma_N = \sigma_0(1 + D/D_0)^{-1/2} + \sigma_R \tag{9}$$

Failure by cracks propagating from V-notches, or cracks running along a bimaterial interface, leads to scaling laws of the general form:

$$\sigma_N = [1 + (D/D_0)^{-2r\lambda}]^{-1/2r} \tag{10}$$

where r = empirical constant close to 1, and parameter λ can be complex or real (Bažant and Le, 2009; Le and Bažant, 2012; Bažant and Le, 2017; Bažant et al., 2021).

Compression fracture of quasibrittle materials typically involves the propagation of compression-shear bands inclined relative to the direction of principal compression stress of the largest magnitude. But the shear crack surface is evident only after the load softens to zero. At maximum load, instead of a shear slip plane, the shear band consists mainly of a series of axial splitting into parallel microslabs that undergo buckling. The buckling mechanism causes the large-size asymptotic scaling law to have a different exponent (c_0, c_1 = constants) (Bažant, 2003):

$$\sigma_N = c_0 + c_1 D^{-2/5} \tag{11}$$

The same law has been obtained for the breakout of deep boreholes (Bažant et al., 1993), based on analyzing an elliptical enlargement of the borehole and applying Eshelby's theorem.

An interesting case is the thermal bending fracture in the floating sea ice sheet. It is known to occur preferentially in thick ice plates, which can be up to 6 m thick. At the bottom, the temperature of the ice plate floating on seawater is near 0 °C. After prolonged cooling, typically to −20° to −40 °C, the temperature gradient across the thickness produces a locked-in eigen-moment. This eventually leads to a sudden bending fracture, which then runs dynamically for tens of miles, preferentially through the thickest ice. Analyzing it as a beam on an elastic foundation showed (Bažant, 1992) that, asymptotically, the critical temperature difference across the ice thickness is

$$\Delta T \propto h^{-3/8} \propto l_{cr}^{-1/2} \tag{12}$$

where h = ice thickness and l_{cr} = buckling wavelength of the beam on elastic foundation. Note that the thicker the ice, the lower the temperature dradient that makes it fracture (if the temperature profiles are similar).

A surprising result, yet to be verified experimentally, is that the strength of composite girders, typically consisting of a steel I-section beam attached by studs to a top concrete slab, should asymptotically scale as

$$\sigma_N \propto h^{-3/4} \tag{13}$$

The reason is that this is a hierarchical fracture, in which one fracture process is in the subscale of another, and each has its own size effects. One is the pullout and shearing of each stud embedded in the concrete slab, and the other is the propagation of stud failures along the row of studs in the concrete–steel interface.

2.3. Gap test for crack-parallel stress effect, with consequences for fracture mechanics

A major change in fracture mechanics is indicated by the recently discovered gap test (Nguyen et al., 2020b,a), whose set-up is sketched in Fig. 2a. The standard notched three-point-bend beam is installed with suitable gaps above the end supports, and elastoplastic loading pads are installed at the crack mouth. The end gaps are designed so as to engage in contact only after the pad forces reach a near-horizontal yield plateau. The end reactions then drive Mode I fracture growth in presence of a constant crack-parallel compression, σ_{xx}. The advantage is that the structure transits from one statically determinate confiuration to another. The SEL, Eq. (2), remains valid in presence of σ_{xx}, as well as σ_{zz}.

From the maximum loads of the gap tests scaled to various sizes D, one can evaluate, for each σ_{xx}-value, the fracture energy, G_f, by means of the size effect method, Eq. (8), which remains valid even in the presence of σ_{xx}. The measured G_f values are plotted in Fig. 2b and c as functions of $-\sigma_{xx}/\sigma_c$ where σ_c = uniaxial compression strength, for four different materials—concrete, fiber-reinforced concrete, aluminum (to be discussed later), and cross-ply fiber composite (Brockmann and Salviato, 2022) (see Fig. 2c). Note that the effect of crack-parallel stress is large and different for each material. This effect cannot be captured by LEFM, cohesive and other line crack models (nor by peridynamic and phase-field models Bažant et al., 2022b). A realistic tensorial damage constitutive relation is required to simulate an FPZ of finite width (Fig. 2d) (the popular Mazars' volumetric softening cannot predict the gap test response (Mazars, 1981)). The microplane model M7 (Caner et al., 2013; Nguyen et al., 2021a) serves this purpose effectively, and the prediction of its latest version M7 is shown in Fig. 2b and c.

Where in practice does the crack-parallel stress matter? • Shear failure of RC beams and slabs • Cracks in prestressed concrete • Longitudinal crack in pressurized aircraft fuselage • Crack in the casing of a solid-fuel rocket • Shear crack in aircraft wing box, rudder, stabilizer • Fracking, esp. with poromechanical stress transfer from the fluid phase to the solid phase • Sea ice

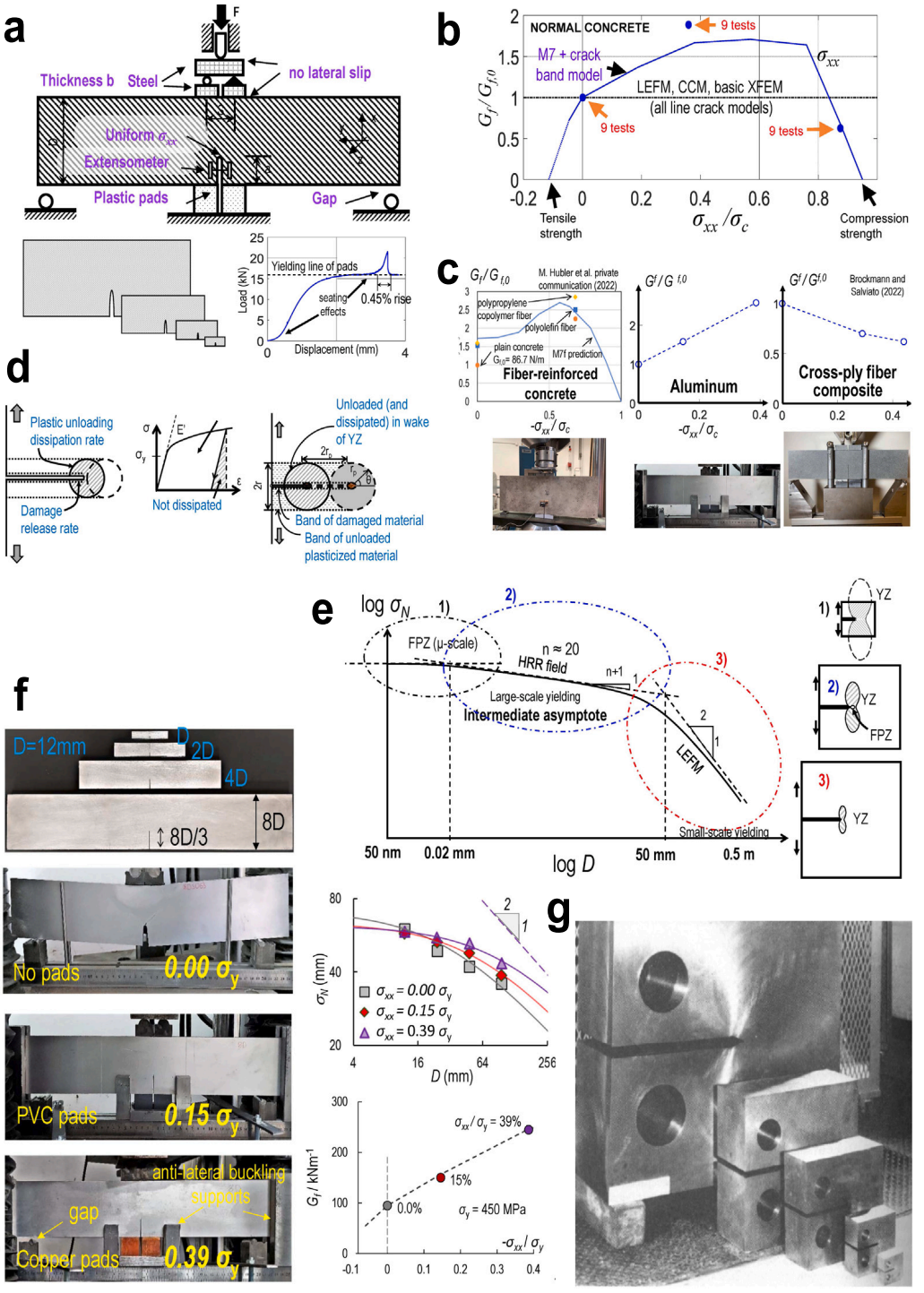

Fig. 2. (a) Gap test set-up, (b) G_f variation with crack-parallel stress of concrete, (c) variation of G_f for different materials (Brockmann and Salviato, 2022), (d) crack growth and FPZ evolution, (e) three asymptotics in hardening metals, (f) gap tests of Al, (g) size effect of Al fracture specimens.

sheet pushing on a fixed structure • Pressure vessel fractures • Fracture in an arch dam or arch bridge abutments, or footings • Crush cans in automobile crashworthiness • Cracks caused by projectile impact and penetration • Cracks in inflatable shells • Most thermal cracks • Cracks in geology, in seismic events, in earthquake fault • Pullout fracture of anchors from rock or concrete • Shear cracks in fiber composite wings, wing box, rudder • Shear crack in fiber composite wind turbine blades •

Particle comminution in projectile impact • Fracture of fatigued plastic-hardening polycrystalline metals • Burst of mine stopes, borehole breakout, failure of tunnel excavations • Fracture of bone, dental materials, annulus hibrosus, other bio-materials, etc.

2.4. Extension of Type 2 scaling to plastic-hardening metals with crack-parallel stress

While polycrystalline plastic-hardening metals have a simpler microstructure than concrete, the scaling of their strength is more intricate, because a millimeter-scale plastic hardening zone surrounds a micrometer-scale fracture process zone. As a consequence, the scaling of structural failure must distinguish three asymptotes, shown in Fig. 2e (Nguyen et al., 2021b).

In contrast to quasibrittle fracture, there is an intermediate asymptote (Nguyen et al., 2021b) (which is a concept due to Barenblatt (1979)); Fig. 2e. This asymptote characterizes the HRR (Rice and Rosengren, 1968; Hutchinson, 1968) field of large-scale yielding in an insufficiently large structure. The slope of the intermediate asymptote is $1/(n+1)$ (Nguyen et al., 2021b) where n is the plastic-hardening exponent of the Ramberg–Osgood uniaxial stress–strain law for metals (where n normally equals 10 to 20).

Matching of the singular elastic field of small-scale yielding for structures of sufficiently large size D to the singular elasto-plastic field for large-scale yielding depends on the crack-parallel stress σ_{xx} and may be approximately determined variationally by the principle of virtual work (this effect, called the T-stress effect, has been known since the 1980s but it was apparently unknown that a part of it must be attributed to the micrometer scale width of the FPZ). The scaling law bridging the FPZ and the small-scale yielding for large D needs again to be based on the energy balance equation (Nguyen et al., 2021b), which now reads:

$$\mathcal{G}_s + \mathcal{G}_b = G_f + G_p \tag{14}$$

Note that there are here two additional terms that do not intervene in our previous analysis of quasibrittle fracture—$\mathcal{G}_b$ which represents the energy released from the band of material traced by the advancing yielding zone, and G_p which represents the energy dissipated in the wake of the yielding zone, which is much wider than the wake of the fracture process zone (Fig. 2d). Interestingly, this leads to an asymptotic matching law of the same form as that for as for concrete, Eq. (2), but its parameters are expressed differently (Nguyen et al., 2021b):

$$\sigma_0^2 = \frac{E' G_f}{2r_p} + \sigma_p^2, \quad D_0 = \frac{2r_p}{g(\alpha_0)} \tag{15}$$

Here r_p = effective radius of the yielding zone, depending on σ_{xx}, and σ_p = yield strength parameter (Nguyen et al., 2021b). Obviously, the modified scaling law can again be used for the size effect method which identifies the fracture energy G_f and the r_p from size effect tests (see Fig. 2f).

The scaling analysis confirmed that, for tests that reach the small-scale yielding, i.e. are well above the transition from the second to the third asymptote, the value of G_f determined in this way is equal to the J-integral (Nguyen et al., 2021b; Bažant et al., 2022a). This fact was, of course, established already in the 1970s, e.g., by the tests at Westinghouse (Fig. 2g, private communication by editor J. Hsia, NTU, Singapore), which showed that, for the largest steel specimen shown, about 0.5 m in size, the standard LEFM testing gave a G_f value that agreed with the ASTM J-integral test based on Rice's J-integral (Rice, 1968) (at that time, there was no interest in scaling laws for solid mechanics, and the data for the specimens of 5 sizes shown in Fig. 2g were not even reported). The scaling law for smaller specimens in the transition from large-scale to small-scale yielding has also been determined (Nguyen et al., 2021b), although its use to determine G_f requires different equations (yet to be published).

2.5. Failure at crack initiation—Type 1 size effect

The Type 1 size effect occurs in structures of initially positive geometry (Bažant et al., 2021) ($[\partial K_I/\partial a]_P > 0$), with no crack or notch, which fail as soon as a macrocrack initiates from a fully formed FPZ (or a fully damaged representative volume element, RVE). In this case, the initial rate of energy release from the structure is independent of D (unlike Type 2).

The Type 1 size effect stems from stress redistribution by the initial FPZ only, and is caused by an increasing ratio of D to the FPZ size. If the material is deterministic, this size effect terminates asymptotically with a horizontal asymptote; if it is not, then with the Weibull scaling law (Fig. 3a). The latter occurs if, and only if, the triggering crack can occur randomly within a large volume of the structure (which is not the case for 3PB specimens). The deterministic size effect that matches the asymptotic properties at both extremes, is given by the formula (Eq. (16)):

$$\sigma_N = \sigma_0 \left(1 + \frac{rD_b}{D}\right)^{1/r} \tag{16}$$

where D_b = constant (transitional size) and r = empirical constant.

Materials are, however, always random, and then (if V_p is large) the size effect of Type 1 transits towards an inclined asymptote of classical Weibull statistical size effect, whose slope is n/m where m = Weibull modulus (for concrete about 24) and n = the number of spatial dimensions. The scaling law, matching the asymptotic behavior at both extremes, is then generalized as Eq. (17):

$$\sigma_N = \sigma_0 \left[\left(\frac{D_b}{D}\right)^{rn/m} + \frac{rD_b}{D}\right]^{1/r} \tag{17}$$

For $m \to \infty$ (no randomness), this equation reduces to the deterministic case.

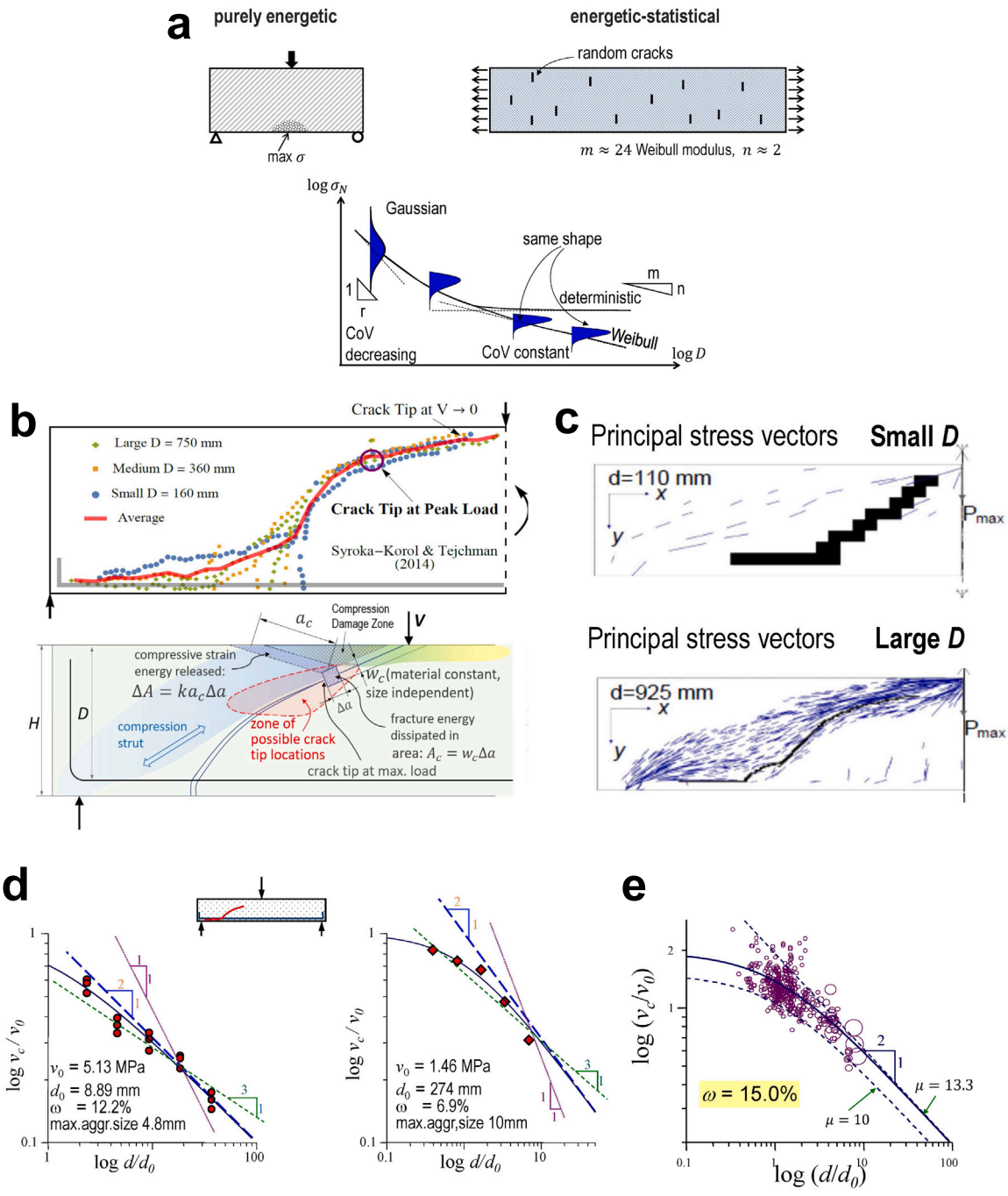

Fig. 3. (a) Type 1 SEL, (b) beam shear mechanism and size effect, (c) variation of the principal stress trajectories of similar geometries, (d) size effect pattern of beam experiments, (e) ACI-445 beam shear database and size effect trend.

However, the statistical size effect can occur only if there is a large zone, V_p, of near maximum stress, as in uniaxial tension or a four-point bend specimen with a long segment of uniform bending moment. For three-point bending, the statistical size effect is negligible because the fracture can initiate at only one place.

2.6. Shear failure of RC beams and slab punching—A quintessential problem of fracture and scaling

This has been a formidable problem, arguably the hardest in fracture mechanics (Fig. 3b). It has been researched for a century, and by fracture mechanics for half century. It caused, or contributed to, sudden failures of many RC structures. Neither LEFM nor cohesive crack model (CCM) can predict it. Why?

The gap test is one explanation. The LEFM or CCM, can predict only the initiation of the main diagonal crack at mid-depth of the beam (see Fig. 3b showing the left part of a beam). But at P_{max}, the maximum load, at which the crack has already grown in a stable manner through about 80% of beam depth, the compressive stress σ_{xx} along the crack (in the shaded blue strip above the main crack), nearly attains the uniaxial compression strength f'_c, and thus reduces the Mode I fracture energy to almost 0, as revealed by the gap test (Nguyen et al., 2020b,a). The failure then proceeds by the propagation of a compression-shear band of splitting cracks across the top of the compression "strut" (Figs. 3b and c), while the triangular wedge above the crack tip (of length a_c) gets pushed up (Yu et al., 2016; Dönmez and Bažant, 2019; Bažant et al., 2022b). Consequently, the Type 2 size effect is followed, and closely so, as confirmed by many tests and explained by strain energy release from the compression "strut" (Fig. 3b), which increases quadratically with the beam size while the energy release from the splitting crack band increases linearly.

The worldwide database of ACI Committee 445, which evolved from a smaller Northwestern database (Bažant and Kim, 1984), now contains about 800 test series collected from the literature (Reineck et al., 2003). The size effect law is best verified by the tests of Syroka-Korol and Tejchman (2014), in which the similarity of failure mode is documented by the coincidence of the dotted curves for three scaled beam sizes plotted in Fig. 3b top in dimensionless coordinates. Figs. 3d and e show examples of comparisons of Type 2 size effect with selected laboratory test data on one concrete only, and with the whole ACI 445 database of many different concretes transformed to Type 2 law coordinates (Reineck et al., 2003). The size effect law of Type 2 for beam shear is now embedded in Standard ACI 318-19 (ACI318, 2019).

The punching shear failure of RC slabs also follows the Type 2 size effect law (Dönmez and Bažant, 2017). This, too, is now codified in ACI 318-19 (ACI318, 2019).

What is the essential cause of the transitional nature of the Type 2 energetic size effect? It is that the total energy release W caused by fracture is a sum of two parts, one growing with the structure size D quadratically (as in LEFM), and one linearly (as in the strength theory); i.e.,

$$W = c_1 D^2 + c_2 l_0 D \tag{18}$$

where l_0 is the material characteristic length and c_1, c_2 are constant (of dimension J/m^2) for geometrically scaled structures.

3. Time

3.1. Creep extrapolation—century plus

Equally serious, albeit different, scaling issues arise for structural durability, especially for concrete structures. In the available worldwide database on creep and shrinkage, containing about 4000 test curves and 65,000 data points, 95% of data are limited to a 6-year duration and nearly all of the rest to a 12-year duration. Accordingly (and perhaps wishfully), the concrete design codes or guides have long specified time curves of creep and shrinkage that flattened off beyond the range of database (even though this was in disagreement with the solidification theory and the theory of microprestress due to disjoining pressure of hindered adsorbed water in nanopores).

What eventually prompted a change was the analysis of the tragic failure the KB Bridge in Palau—a world record prestressed box girder, whose creep deflection reached 1.61 m within 18 years, accompanied by a prestress loss measured as 50% (instead of about 20% as assumed in design); Fig. 4a. Analysis of the deflections (at Northwestern, Bažant et al., 2011b) led to an arduous effort to collect, under the auspices of RILEM TC-MDC, the histories or grossly excessive deflections of large-span bridges. Of the 71 collected (often from reluctant bridge owners) (Bažant et al., 2011a), 28 are displayed in the log–log scales in Fig. 5 (Bažant et al., 2011a), The data on creep compliance of the concretes used were then inferred by inverse analysis, as shown in Fig. 4c.

These data agreed with (though could not prove) the theoretical result that the creep of concrete at constant stress proceeds roughly logarithmically in time, without any bound, doubtless for over a century, as introduced in RILEM Model B3 (Bažant and Baweja, 1995a,b). After this demonstration, the ACI-209 guidelines as well as the European *fib* Model Code were changed promptly (Fig. 4b).

3.2. Scaling of shrinkage and its extrapolation via two-sided asymptotic matching

Drying shrinkage, ϵ_{sh}, is caused by a decrease in the surface energy of the pores. At constant temperature, T, ϵ_{sh} is a function of the chemical potential, $\mu(h)$, of pore water, which represents the Gibbs free energy per unit mass. The drying shrinkage, as well as the effect of drying on creep, is controlled by the diffusion of water through unsaturated concrete. The diffusion is highly nonlinear due to a two-orders-of-magnitude drop of diffusivity and permeability as pore humidity h decreases (Bažant and Jirásek, 2018). However, the asymptotic properties are simple. The average shrinkage strain, $\bar{\epsilon}_{sh}(\hat{t})$, in a test cylinder was shown to be approximately proportional to the total water loss, even though the diffusion problem is highly nonlinear. For similar cross sections

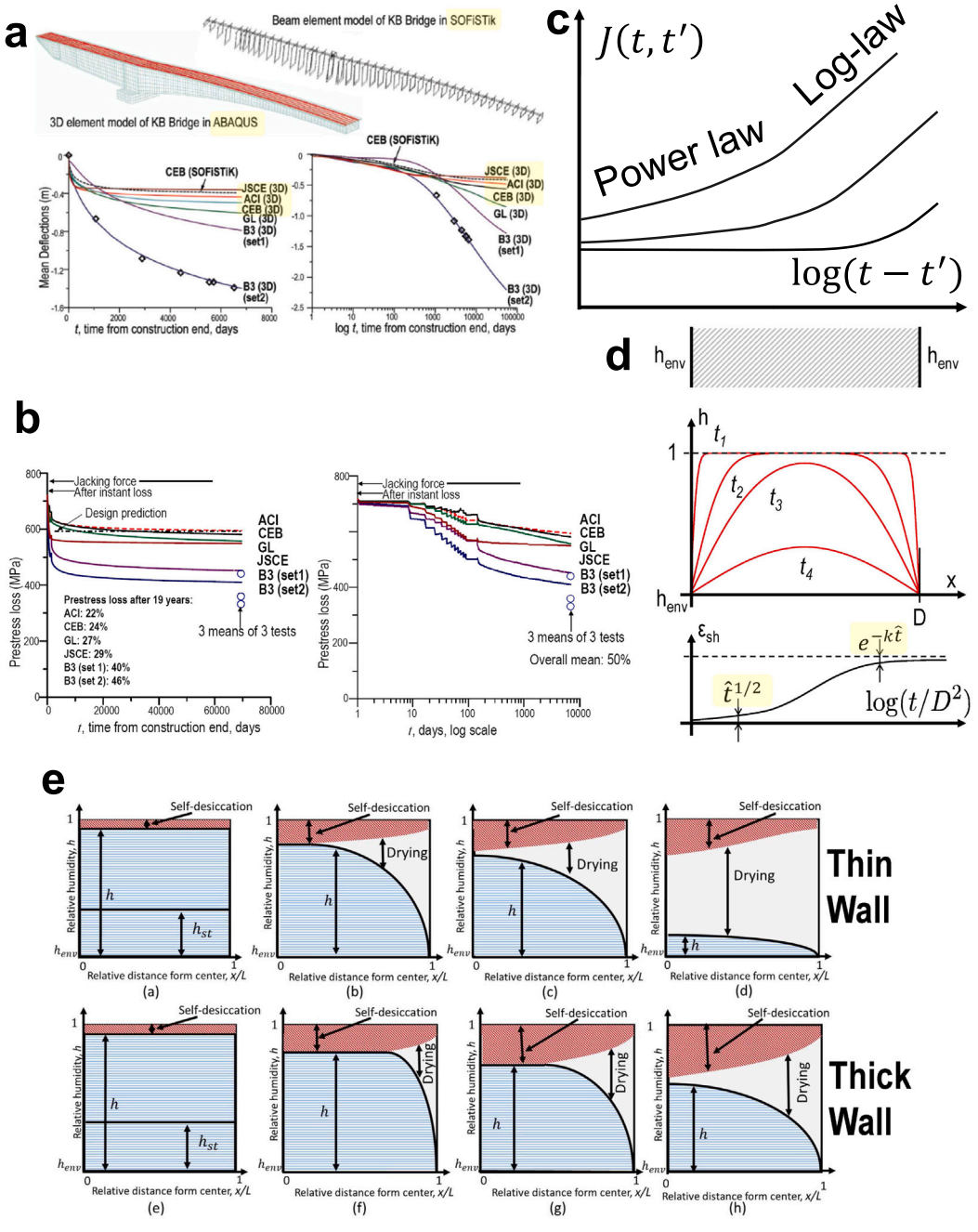

Fig. 4. (a) Deflection predictions of KB Bridge in Palau, (b) predictions of prestress loss of KB Bridge, (c) evolution of compliance function with time, (d) drying front pattern on depth section of a wall, (e) four different pore humidity profiles for both thin and thick walls.

of characteristic size D, despite nonlinear diffusivity, the diffusion theory shows that the pore water content generally evolves as a function of the effective time:

$$\hat{t} = \frac{1}{c}\left(\frac{t}{D^2}\right) \tag{19}$$

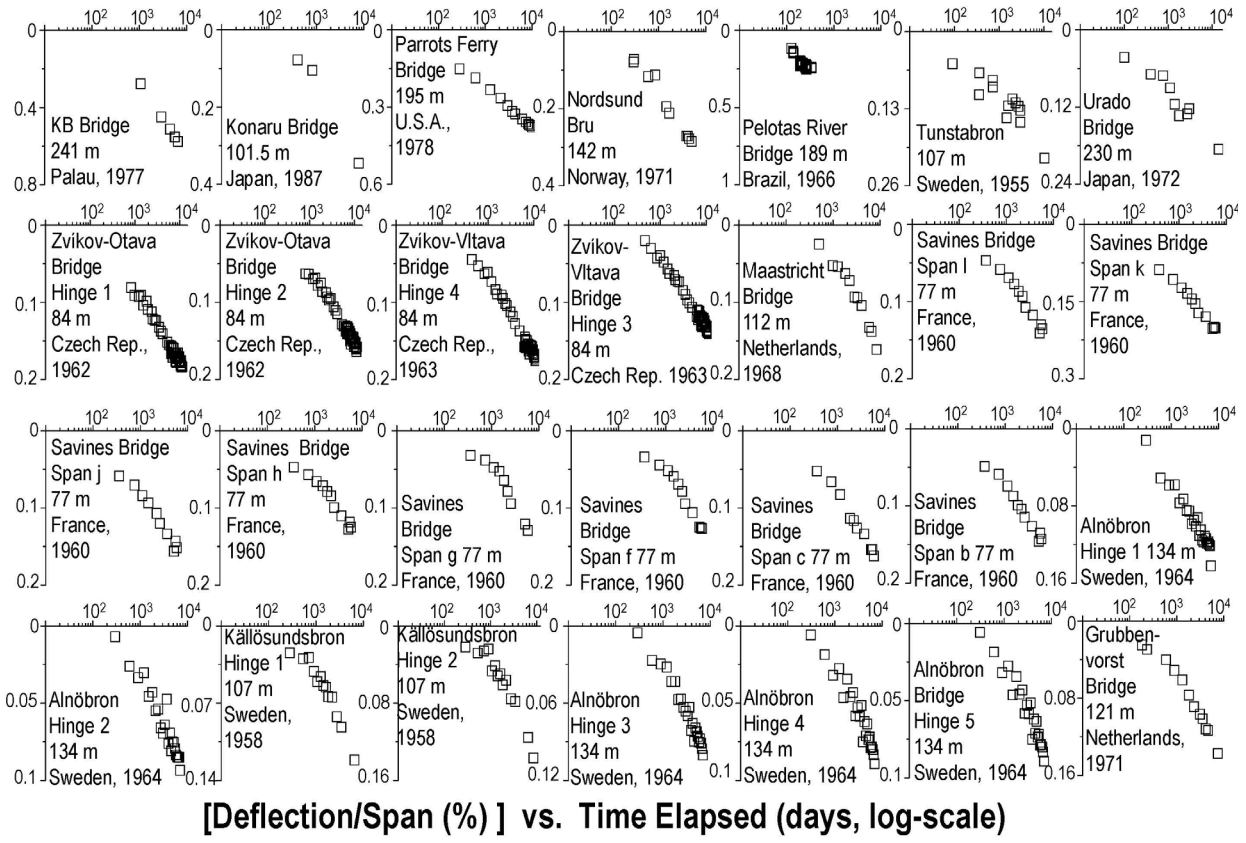

Fig. 5. Computed deflections of the 28 current bridges around the world.

where t = actual time measured from the instant of exposure to drying in a steady environment (c= constant). A typical pore humidity profile at the drying profile is illustrated in Fig. 4d for a slab section. Fig. 4e depicts how the interaction of evolving humidity profiles due to drying and selfdesiccation depends on specimen thickness.

It can be shown that, asymptotically for short $\hat{t}$ (i.e., for $t \to 0$ or $D \to \infty$), the water content of a drying specimen evolves as $\sqrt{\hat{t}}$, and asymptotically for very long $\hat{t}$ (i.e., for $t \to \infty$ or $D \to 0$) should approach a final value exponentially. These theoretically established opposite asymptotic properties, can all be bridged by the function (Eq. (20)):

$$\epsilon_{sh}(\hat{t}) = \epsilon_\infty S(t), \quad \text{where} \quad S(t) = \tanh\sqrt{\hat{t}} \tag{20}$$

where ϵ_∞ is a constant (this formula is embodied in RILEM standard recommendations, models B3 (Bažant and Baweja, 1995a,b) and B4 (Wendner et al., 2013; Hubler et al., 2015), endorsed by ACI-209 committee).

This formula, however, is sufficient only for old concretes with high water–cement ratios ($w/c > 0.5$), in which the selfdesiccation was feeble, terminating at pore relative humidity $h \approx 0.98$. Modern concretes, characterized by a halved cement content and a very low water–cement ratios (as low as 0.25) develop large selfdesiccation due to the chemical process of hydration, which can reach as low $h = 0.65$. Such selfdesiccation produces major autogenous shrinkage, $\epsilon_{au}(t_e)$, driven by selfdesiccation, of similar magnitude as the drying shrinkage, ϵ_{sh}; t_e is the effective hydration period (also called the maturity). Based on plots in a linear time scale, which are misleading, the autogenous shrinkage was assumed to terminate within a few months, but the collection of extensive data shown in Fig. 6a confirmed that the autogenous shrinkage of sealed specimens evolves as a power law of exponent about 0.2, probably over the at least a century.

The interaction of autogenous and drying shrinkage, depicted in Fig. 4e by four subsequent pore humidity profiles for thin and thick walls, brings about further complexity. The rate of selfdesiccation, and thus of autogenous shrinkage, decreases drastically with a decrease of pore humidity. Therefore, in thin slabs, which dry relatively quickly, the autogenous shrinkage plays a small role, but in relatively thick ones a major role.

Similar is the interaction with wetting in water submersion. Prior selfdesiccation in the cores of specimens under water produces much pore space for imbibing more water. In thin specimens the autogenous shrinkage is soon overpowered by the wetting front and, except for a short initial period, the specimen swells (i.e., the average shrinkage strain is positive). But thick specimens undergo autogenous shrinkage for a long time even underwater, as long as the wetting front penetrates only a small part of specimen thickness D.

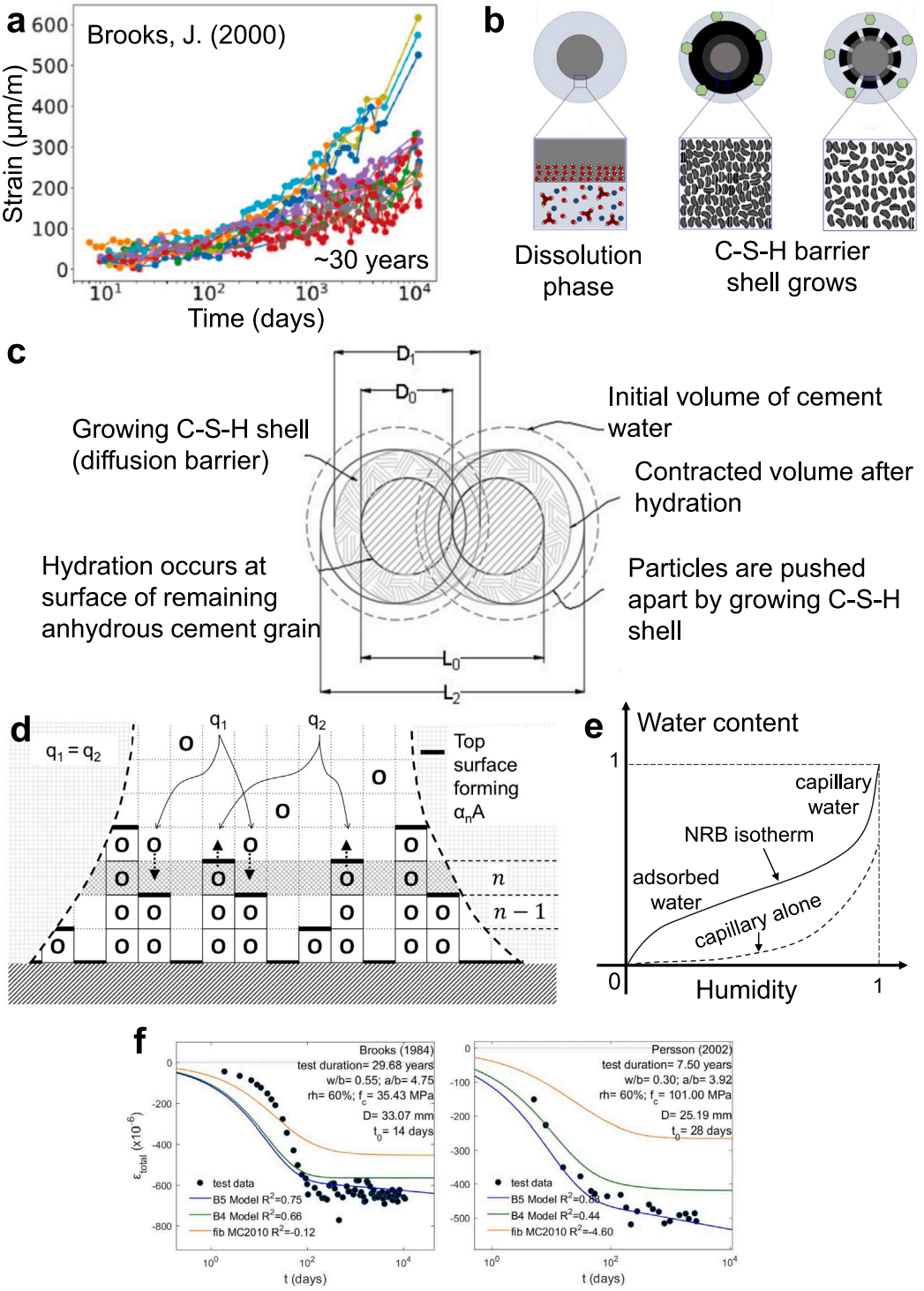

Fig. 6. (a) 30-year autogenous shrinkage tests, (b) hydration growth with C–S–H barrier theory, (c) hydration mechanism of cement grains, (d) internal humidity profile, (e) sorption isotherm, (f) long-term drying shrinkage evolution with the asymptotic matching equation.

The problem is complex but one may again exploit the asymptotics; 8 asymptotic properties of two shrinkage-driving processes, 4 for the external drying and 4 for the selfdesiccation, are known at $t \to 0, t \to \infty, D \to 0, D \to \infty$. They can be introduced by the

functions

$$f_h(t) = k_h S(\hat{t}), \quad f_w = k_w S_w(\hat{t}) \quad \text{where} \quad \hat{t} = t/D^2 \tag{21}$$

The following formula for the total stress-independent strain has all the required asymptotic properties:

$$\epsilon(t) = \underbrace{\epsilon_{sh,\infty} f_h(\hat{t}) + [1 - f_h(\hat{t})]\epsilon_{au}(t)}_{1st\ matching}\underbrace{[1 - f_w(t)] + \epsilon_{sw}(t)_\infty f_w(t)}_{2nd\ matching} \tag{22}$$

The first, as well as the second under-braced term, has the form of interpolation by the partition of unity, with partition factors f_h and $(1 - f_h)$. The second and third terms of the sum have also the form of partition of unity, with partition factors $[1 - f_w]$ and f_w. However, these partitions of unity actually represent functions $f_h(\hat{t})$ and $f_w(\hat{t})$ and thus include not just interpolations but quadruple asymptotic matching, since functions $f_h(\hat{t})$ and $f_w(\hat{t})$ already include the asymptotic properties. For a great variety of concretes, Eq. (22) allowed a big improvement of the fits of the test data on shrinkage and swelling; see the example in Fig. 6f.

The asymptotic term $\epsilon_{sw}(t)$ in the last equation includes the expansion of solidified cement due to hydration. The notion of expansion might seem heretical because the chemical reaction of hydration has been known since 1877 to be contractive (Le Chatelier, 1887), i.e., the nano-powdered hydrated cement to have a smaller volume than the anhydrous cement and the water needed for its hydration. However, a hydrating cement forms a porous solid skeleton, in which the shells of the hydration product, the C–S–H, envelop the cement particles and tend to push them apart as they grow (Figs. 6b–c) (in similarity to crystal growth pressure). This is a process proceeding at a declining rate for days and decades, causing gradual expansion of the skeleton, superposed on other deformations.

Asymptotic aspects of sorption isotherm

The analysis of water diffusion in concrete requires knowing the sorption isotherm, i.e., the variation of pore water content w as a function of relative humidity h in the pores, at a constant temperature. The BET (Brunauer, Emmett, Teller (Brunauer et al., 1938)) isotherm has generally been used, but it cannot capture the adsorption range with a correct low h asymptotics and is asymptotically incorrect for $h \to 1$. Recently, the classical statistical derivation of this isotherm has been made more realistic to capture the fact that, as the nanopores are getting filled at increasing h, the surface of the multi-molecular adsorption layers that is exposed to vapor diminishes, roughly as a power function of adsorption layer thickness (Nguyen et al., 2019, 2020).

Introducing this restriction into the statistics, or frequency, of water molecule condensation and evaporation rates (Fig. 6d), one gets a recursive equation for rates q_1 and q_2 of condensation and evaporation, leading to a sum of water contents from one to an infinite number of water layers. This sum can be evaluated in terms of the Jonquière special function, Li. Then, noting that not more than five layers can get adsorbed, a similar sum from six to infinity is excluded, which allows this isotherm, unlike BET, to be asymptotically correct not only for $h \to 0$ but also for $h \to 1$, giving a finite water content at $h = 1$ (Fig. 6e). The new isotherm, labeled NRB (Nguyen et al., 2019), reads:

$$\theta(h,T) = \frac{\mathrm{Li}_{q-1}(h)}{c_T^{-1} + \mathrm{Li}_q(h)} \tag{23}$$

where c_T = temperature dependent parameter, and θ = relative saturation of the nanoporous material, e.g., concrete.

4. Risk

Experts generally agree that, a tolerable failure probability in the design of engineering structures, such as bridges, aircraft, and computers, should not exceed 10^{-6}, or one in a million, which is in the US the probability of being killed by lightning, a falling tree or wild animal. To verify it experimentally, a structure or material test would have to be repeated 10^7-times, which is impossible. This is a tough problem since for the commonly assumed probability distributions such as normal (or Gaussian) and Weibullian, which can hardly be distinguished from each other in the central range of probabilities > 1% (Fig. 7a), the distances from the mean to the point of 10^{-6} differ as about 2 : 1. The correct distribution can be anywhere in between. Experiments alone are useless. They must be aided by a physically based theory as the asymptotic support.

It has long been thought that the theory of random material flaws is the answer, but it is not. It is not wrong but merely replaces one set of hypotheses with another, and is a sort of circular argument. The answer must be sought at the nanoscale. Failure always involves the breakage of interatomic bonds, which follows Kramers' rule of atomistic transition rate theory; see Fig. 7b. The important point is that, at the atomic scale, the failure frequency is also the probability. The bond ruptures and restorations occur at different rates depending on their activation energy barriers, which are biased by the applied stress. From this analysis, one concludes (Bažant and Pang, 2007; Bažant et al., 2021) that the tail of the probability density function (pdf) of failure probability P_f on the nanoscale is a power law of applied stress with exponent 2 (given that the Péclet number of the relevant Fokker–Planck equation is > 4).

The transition from the nanoscale to the material scale (7 orders of magnitude in concrete) can be modeled as an alternation of series and parallel couplings, imagined to act at each scale across and along the fracture process zones (Figs. 7c–d). Asymptotic analysis shows that the power law tail is indestructible but its exponent increases from 2 to about 20 to 40.

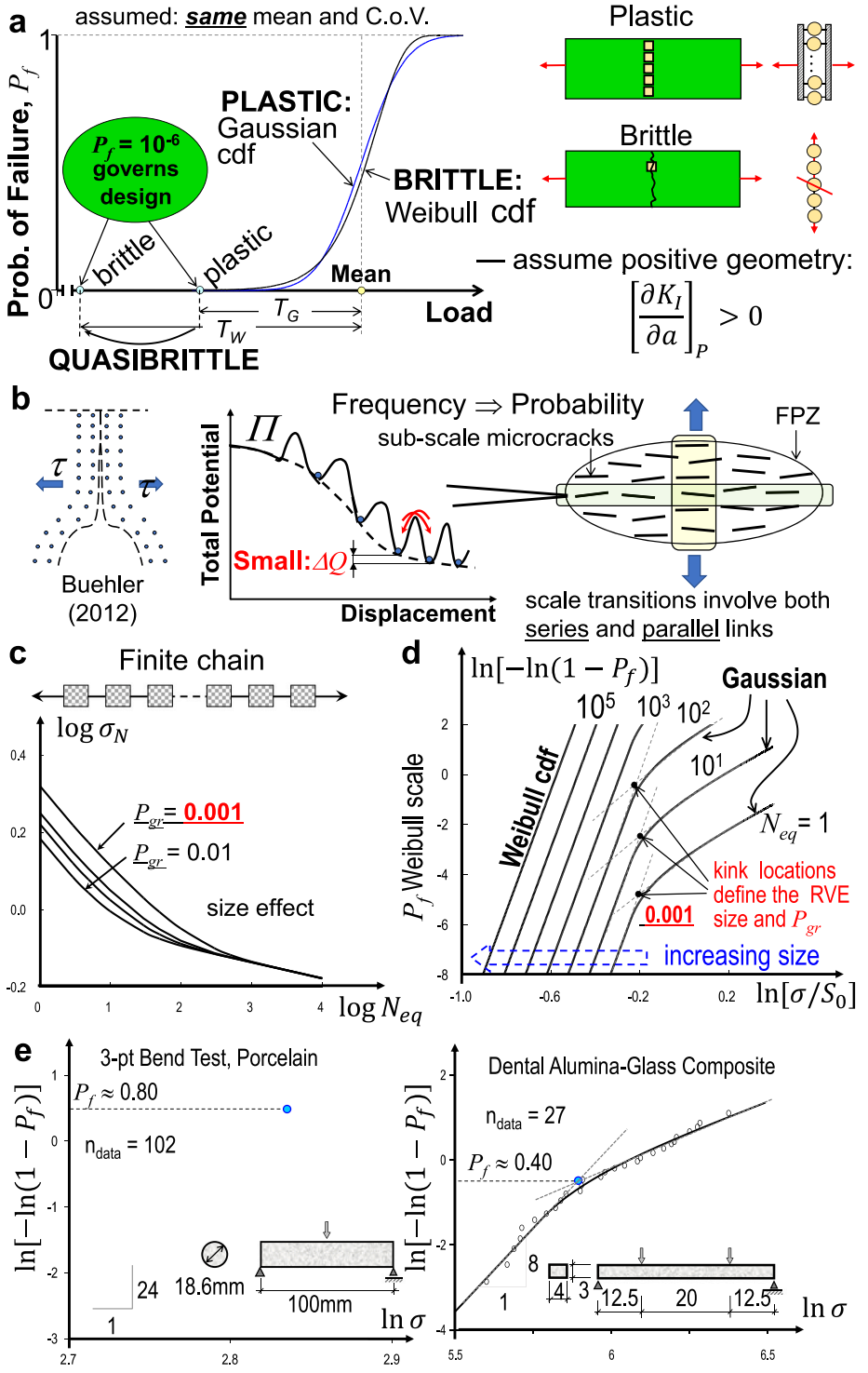

Fig. 7. (a) Central range of probabilities, (b) breakage of interatomic bonds, (c), (d) alternation of parallel couplings, (e) Gauss–Weibull distributions of porcelain and Al-Glass composite.

The result is that larger quasibrittle structures can be modeled as a chain (i.e., a series coupling, with each link corresponding to one RVE (representative volume element)). The links are characterized by a pdf with a power law tail. If the number N of links were infinite, the pdf of structural failure would be Weibullian. An important new point (Bažant and Pang, 2007) was that, for quasibrittle

structures, the number, N, of links is finite, because the fracture process zone is not small enough. This causes a Weibullian core to transit at higher probabilities (and stress $\to \infty$) to a Gaussian tail, and the Gauss–Weibull pdf represents an asymptotic matching of these two limiting behaviors (Bažant et al., 2021; Le et al., 2011; Bažant and Le, 2017). Some of the experimental verifications of the Gauss–Weibull distribution are shown in Fig. 7e (Bažant et al., 2009), and Fig. 8a demonstrates generalizations to fatigue lifetimes. The distributions are plotted in these figures in the Weibull scale, which is a scale in which the Weibull distribution appears as a straight line.

For a long time, the deviations to the right were attributed to the existence of a finite threshold (leading to a 3 parameter Weibull distribution), which has been shown to be incorrect and misleading. This is confirmed by a grossly incorrect size effect, which is caused by the presence of a finite threshold; Figs. 8b–c.

The foregoing discussion pertains to particulate materials such as concrete. Of great interest are more intricate material architectures such as that of nacre, whose essence is a "brick-and-mortar" arrangement of nano-platelets of aragonite ($CaCO_3$), which obviously does not fit the weakest-link chain model. But it also does not fit the fiber bundle (parallel coupling) model. These two models, sketched in Fig. 8d, were until 2017 the only two probabilistic failure models for which the calculation of the exact pdf, including the far-left tail, was feasible. In 2017 it was found (Luo and Bažant, 2017) that the failure probability of nacre is captured by the "fishnet" model (see Fig. 8e), which is the third analytically tractable model, and resembles a fishnet pulled diagonally. The distinct feature of the fishnet model is that it represents a regular alternation of parallel and series links while its pdf can also be solved exactly (Luo and Bažant, 2017).

Rectangular fishnets have a useful new property. As their width-to-length aspect ratio, W/L, changes from 0 to ∞, they display a continuous transition from Gaussian distribution to Weibull distribution. They are the only known physical model to accomplish that.

The failure probability, P_f, of a fishnet can be regarded as a sum of P_{fi} $(i = 1, 2, \ldots)$ of the cases (disjoint sets) in which the failure is caused by 1, 2, 3, ... or n link failures. For up to 3, an exact analytical solution of P_f has been found (Luo and Bažant, 2017), and for up to about 1000 links in the fishnet, this solution is almost exact for any n. These curves have been confirmed by one million Monte Carlo simulations per probability distribution curve (so each point represents an aggregation of about 10,000 Monte Carlo simulations (Fig. 8f, Fig. 9a)). If we denote σ = uniaxial uniform tensile stress applied and f_i = mean strength of each link and m its Weibull modulus, Fig. 8f shows in Weibull scale the probability distributions for 1, 2, 3, ... n links failed at maximum load, P_{max}. The case $m = 1$ is the Weibull distribution (weakest-link model). What is revealing for material architecture design is that the combination of series and parallel links provides an enormous (40%) increase of strength at $P_f = 10^{-6}$, compared to the weakest-link model.

As marked in Fig. 8f, the probability curves in the Weibull scale of coordinates $Y = \ln[-\ln(1 - P_f)]$ versus $X = \ln\sigma$ represent envelopes to asymptotic slopes $m, 2m, 3m, \ldots$. It was found that they may be described by a simple differential equation:

$$\frac{dY}{dX} = m_0 + m_1 Y \quad \text{with} \quad P_f = 1 - e^{-e^{-Y}} \tag{24}$$

which is easily solved by the separation of variables. This equation captures not only the increase of slope while moving down at fixed N to lower probability but also the increase of slope at median probability 0.5 in Fig. 9a while moving left toward larger geometrically similar fishnets, requiring a progressively larger number N of links to fail before P_{max}.

The question is whether this trend may continue to very large N. It cannot. For a fishnet with $N = 10^5$ links, intuition suggests, and computations indicate, that often many, say 20, links in a row need to fail to reach P_{max} and cause overall failure. Such a row effectively represents a crack, with singular stress concentrations at its ends, which does not exist for low N. But it is not a crack in an elastic continuum. It was shown that the continuum limit of an elastic fishnet is simply the Laplace equation. The solution of this equation via complex potentials showed that a crack in a rectangular domain represents a positive geometry (Bažant et al., 2021), which means that at a certain critical length (at which the energy release rate balances the dissipation) it will cause dynamic failure.

Because, in a uniformly stressed big fishnet, such a crack may occur at many possible random locations, the behavior of big fishnet must approach that of the weakest-link model and, because of the power-law tail, this implies that for $N \to \infty$ the sequence of probability distribution curves in Fig. 9a must eventually approach a straight line representing Weibull distribution, whose slope is much larger than m, perhaps $3m$ (studies are still under way, joint with Prof. J.-L. Le, University of Minnesota, and Houlin Xu, at Northwestern). The transition from small to large fishnets, i.e., from fishnet distribution to Weibull distribution, represents a problem of asymptotic matching, facilitated by Eq. (24).

What if the fishnet links, instead of breaking suddenly, exhibit progressive postpeak softening? This has been handled by representing the softening as a progression of small stress drops (Luo and Bažant, 2020), which leads to Pólya-Aeppli geometric Poisson distribution. The results are overall quite similar (Luo and Bažant, 2018).

The fishnet model has been generalized to three dimensions and applied to the octet material architecture (Fig. 9b), which can nowadays be easily created by 3D printing. Their deterministic analysis (e.g., Zhang et al., 2019) confirmed that this architecture offers a very high strength-to-weight ratio. A probabilistic analysis similar to fishnet (Luo and Bažant, 2020) showed that the safety margin of an octet structure at $P_f = 10^{-6}$ is even greater than it is for a 2D fishnet.

The fracture of plain concrete specimens in tension has been assumed to follow the series-coupling (or weakest-link) model. However, recent simulations of force chains in tension of small specimens (i.e., not large enough compared to the inhomogeneity size) showed that the force chains are not parallel but connect laterally (see Fig. 9c). This suggests that, for small structures below the LEFM size range, the series coupling model of failure probability may have to be enriched by some small percentage of parallel couplings.

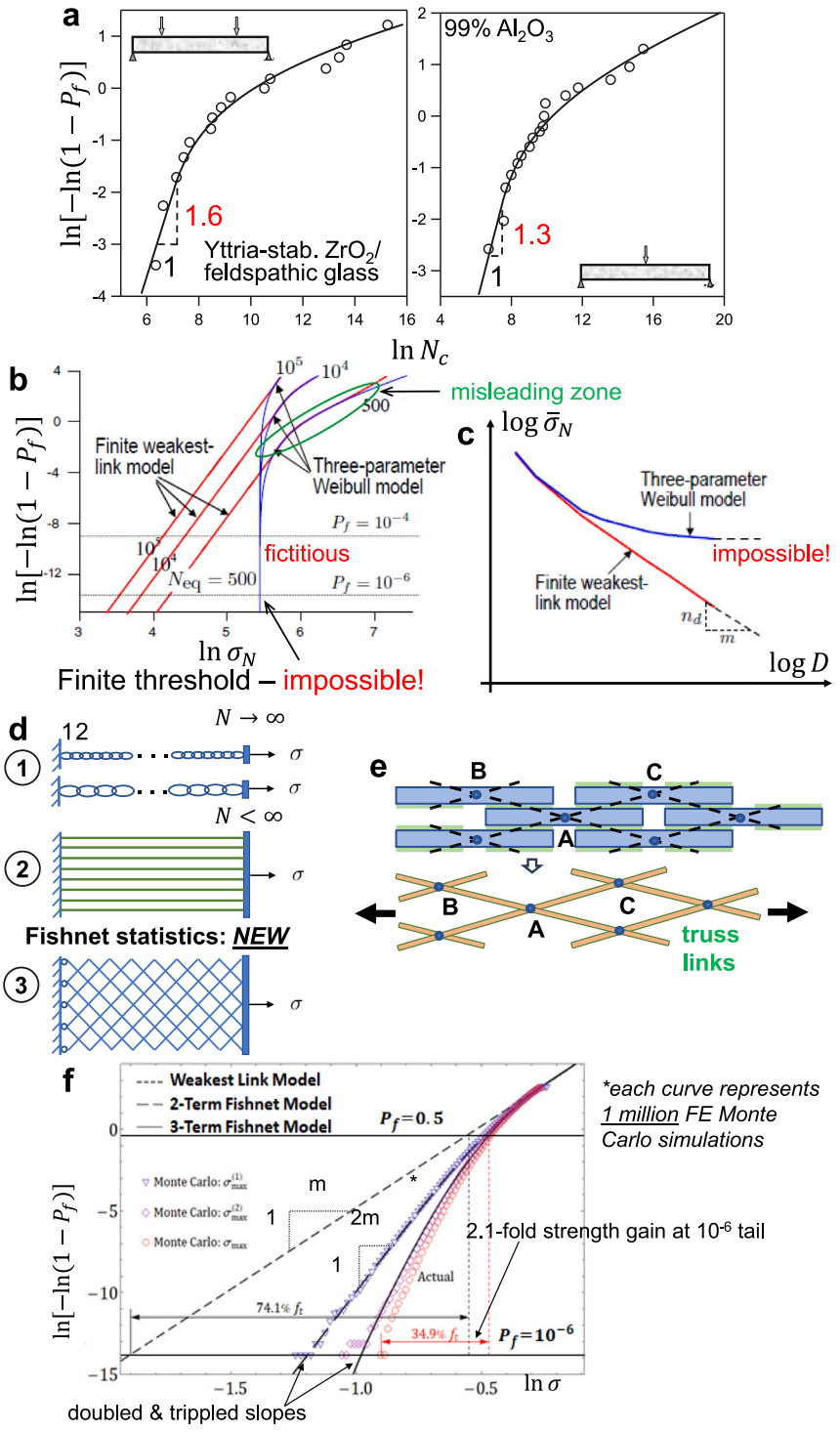

Fig. 8. Illustrations of the Fishnet statistics.

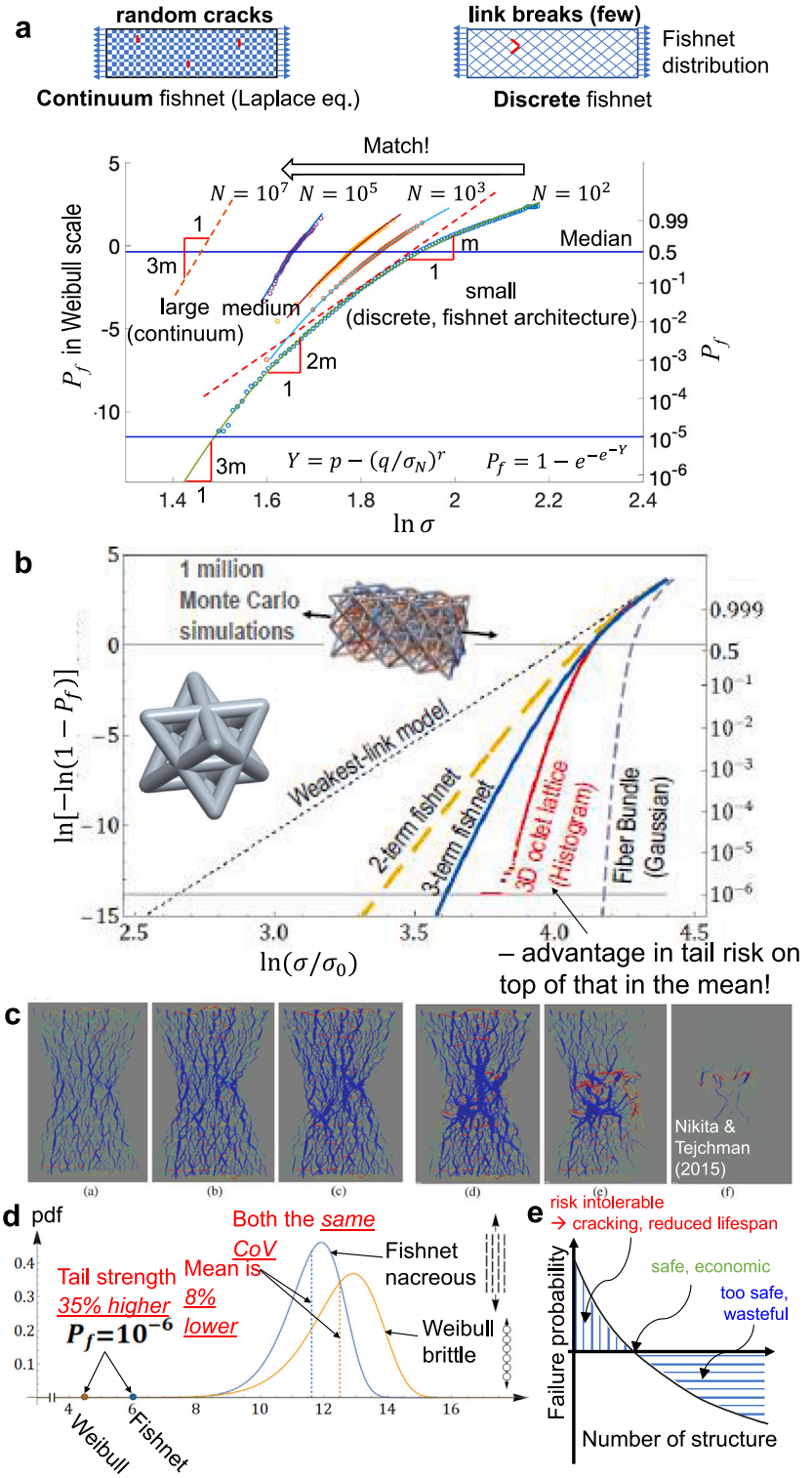

Fig. 9. (a) Continuum and discrete Fishnet statistics, (b) three-dimensional generalization of the Fishnet model, (c) illustration of the force chain connections (Nitka and Tejchman, 2015), (d) effect of material architecture on failure probabilities, (e) safety margins of the structures.

The complex effect of material architecture on P_f calls for caution in creating and appraising new materials. It has been demonstrated that material A, whose mean strength is 8% lower than that of material B, can be at failure probability level 10^{-6}

35% stronger than material B (Fig. 9d). The latter is what normally matters for the design more than the mean strength, and so material A is what should be used.

5. Closing comments on broader implications

The problems of big extrapolations highlighted here affect many engineering fields but are endemic in concrete engineering. Aside from safety and economic aspects, a wrong or poor extrapolation has an enormous environmental impact, particularly on CO_2 emissions.

The CO_2 emissions from cement production currently equal those from all the cars and trucks in the world and, unlike the latter, are on a steep upward trajectory even though the cement content of concrete has already been reduced to about one-half during the last four decades. Efforts are being made to modify cement and its production (e.g., by calcined clay), but no major breakthrough is yet in sight. One aspect, though, has not even received sufficient attention—the causes of inadequate durability.

Although the lifetimes of major structures such as bridges are supposed to be at least a century, major repairs or replacements are nowadays necessary within 20 to 40 years; likewise for pavements. If the lifetimes could be doubled, the demand for cement would drop significantly in the long run. What is the cause of insufficient durability? In most cases, it is various types of corrosion or degradation processes. But it must be noted that virtually all these processes (even ASR) get triggered by excessive cracking or fracture, leading to the ingress of water and corrosive agents. No cracking—no corrosion.

Misprediction of long term creep and shrinkage—a problem of extrapolation in time as well as size—is one obvious frequent cause of excessive distributed cracking and localized fracture. But it is generally overlooked that both excessive and insufficient safety factors—a problem of probability extrapolation—are, too.

As sketched in Fig. 9e, only a few concrete structures happen to have the correct safety, providing failure probability 10^{-6}. The spectrum of all concrete structures includes those with insufficient overall safety factors and others with excessive ones. Note that both lead to wasteful use of concrete, and thus both increase CO_2 emissions. When the safety factor is too high, too much concrete is used. This leads not only to a financial loss but also to increase of CO_2 emissions. When it is too low, cracking likely develops, shortening the lifetime, which in turn increases the demand for concrete, and thus the CO_2 imprint, in the long run.

Declaration of competing interest

The authors declare that they have no known competing financial interests or personal relationships that could have appeared to influence the work reported in this paper.

Data availability

Data will be made available on request.

Acknowledgments

Partial financial support, under National Science Foundation, United States of America grant CMMI-202964 and ARO, United States of America Grant W911 NF-19-1-0039, both to Northwestern University, are gratefully acknowledged.

References

ACI318, 2019. Building Code Requirements for Structural Concrete and Commentary. American Concrete Institute, Farmington Hills.
Alfredo, H., Tang, W.H., 1984. Probability Concepts in Engineering. Vol. 2, John Wiley and Sons.
Askarinejad, S., Rahbar, N., 2015. Toughening mechanisms in bioinspired multilayered materials. J. R. Soc. Interface 12 (102), 20140855.
Barenblatt, G.I., 1979. Similarity, Self-Similarity, and Intermediate Asymptotics. Consultants Bureau, New York.
Barenblatt, G.I., 2003. Scaling. Vol. 34, Cambridge University Press.
Bažant, Z.P., 1984. Size effect in blunt fracture: concrete, rock, metal. J. Eng. Mech. 110 (4), 518–535.
Bažant, Z.P., 1990. Size-effect method for determining fracture energy and process zone size of concrete. Mater. Struct. 23, 461–465.
Bažant, Z.P., 1992. Large-scale thermal bending fracture of sea ice plates. J. Geophys. Res. Oceans 97 (C11), 17739–17751.
Bažant, Z.P., 2002. Scaling of Structural Strength. CRC Press.
Bažant, Z.P., 2003. Shear buckling of sandwich, fiber composite and lattice columns, bearings, and helical springs: Paradox resolved. J. Appl. Mech. 70 (1), 75–83.
Bažant, Z.P., Baweja, S., 1995a. Justification and refinements of model B3 for concrete creep and shrinkage-1. Statistics and sensitivity. Mater. Struct. 28 (7), 415–430.
Bažant, Z.P., Baweja, S., 1995b. Justification and refinements of model B3 for concrete creep and shrinkage 2. Updating and theoretical basis. Mater. Struct. 28 (8), 488–495.
Bažant, Z.P., Dönmez, A.A., Nguyen, H.T., 2022a. Précis of gap test results requiring reappraisal of line crack and phase-field models of fracture mechanics. Eng. Struct. 250, 113285.
Bažant, Z.P., Hubler, M.H., Yu, Q., 2011a. Excessive creep deflections: An awakening. Concr. Int. 8 (33), 44–46.
Bažant, Z.P., Hubler, M.H., Yu, Q., 2011b. Pervasiveness of excessive segmental bridge deflections: Wake-up call for creep. ACI Struct. J. 108 (6), 766.
Bažant, Z.P., Jirásek, M., 2018. Creep and Hygrothermal Effects in Concrete Structures. 1st Ed., Springer.
Bažant, Z.P., Kazemi, M.T., 1991. Size effect on diagonal shear failure of beams without stirrups. ACI Struct. J. 88 (3), 268–276.
Bažant, Z.P., Kazemi, M., et al., 1990. Determination of fracture energy, process zone length and brittleness number from size effect, with application to rock and conerete. Int. J. Fract. 44 (2), 111–131.
Bažant, Z.P., Kim, J.-K., 1984. Size effect in shear failure of longitudinally reinforced beams. ACI J..

Bažant, Z.P., Kim, J.-J.H., Daniel, I.M., Becq-Giraudon, E., Zi, G., 1999. Size effect on compression strength of fiber composites failing by kink band propagation. Int. J. Fract. 95 (1), 103–141.
Bažant, Z.P., Le, J.-L., 2009. Nano-mechanics based modeling of lifetime distribution of quasibrittle structures. Eng. Fail. Anal. 16 (8), 2521–2529.
Bažant, Z.P., Le, J.-L., 2017. Probabilistic Mechanics of Quasibrittle Structures: Strength, Lifetime, and Size Effect. Cambridge University Press.
Bažant, Z.P., Le, J.-L., Bazant, M.Z., 2009. Scaling of strength and lifetime probability distributions of quasibrittle structures based on atomistic fracture mechanics. Proc. Natl. Acad. Sci. 106 (28), 11484–11489.
Bažant, Z.P., Le, J.-L., Salviato, M., 2021. Quasibrittle Fracture Mechanics and Size Effect: A First Course. Oxford University Press.
Bažant, Z.P., Lin, F.-B., Lippmann, H., 1993. Fracture energy release and size effect in borehole breakout. Int. J. Numer. Anal. Methods Geomech. 17 (1), 1–14.
Bažant, Z.P., Nguyen, H.T., Abdullah Dönmez, A., 2022b. Critical comparison of phase-field, peridynamics, and crack band model M7 in light of gap test and classical fracture tests. J. Appl. Mech. 89 (6), 061008.
Bažant, Z.P., Oh, B.H., 1983. Crack band theory for fracture of concrete. Matériaux Et Construction 16 (3), 155–177.
Bažant, Z.P., Pang, S.-D., 2007. Activation energy based extreme value statistics and size effect in brittle and quasibrittle fracture. J. Mech. Phys. Solids 55 (1), 91–131.
Bažant, Z.P., Planas, J., 2019. Fracture and Size Effect in Concrete and Other Quasibrittle Materials. Routledge.
Brockmann, J., Salviato, M., 2022. The gap test: effects of crack parallel compression on fracture in carbon fiber composites. arXiv preprint arXiv:2207.12649.
Brunauer, S., Emmett, P.T., Teller, E., 1938. Adsorption of gases in multimolecular layers. J. Am. Chem. Soc. 60, 309–319.
Budiansky, B., Fleck, N.A., 1993. Compressive failure of fibre composites. J. Mech. Phys. Solids 41 (1), 183–211.
Caner, F.C., Bažant, Z.P., ASCE, H.M., 2013. Microplane model M7 for plain concrete. I: Formulation. J. Engrg. Mech. 139 (12).
Charles, R., 1958. Static fatigue of glass. I. J. Appl. Phys. 29 (11), 1549–1553.
Chen, L., Ballarini, R., Kahn, H., Heuer, A., 2007. Bioinspired micro-composite structure. J. Mater. Res. 22 (1), 124–131.
Coleman, B.D., 1957. Time dependence of mechanical breakdown in bundles of fibers. I. Constant total load. J. Appl. Phys. 28 (9), 1058–1064.
Coleman, B.D., 1958. Statistics and time dependence of mechanical breakdown in fibers. J. Appl. Phys. 29 (6), 968–983.
Cusatis, G., Schauffert, E.A., 2009. Cohesive crack analysis of size effect. Eng. Fract. Mech. 76 (14), 2163–2173.
Daniels, H.E., 1945. The statistical theory of the strength of bundles of threads. I. Proc. R. Soc. Lond. Ser. A Math. Phys. Eng. Sci. 183 (995), 405–435.
Di Luzio, G., Cusatis, G., 2018. Cohesive crack analysis of size effect for samples with blunt notches and generalized size effect curve for quasi-brittle materials. Eng. Fract. Mech. 204, 15–28.
Dönmez, A., Bažant, Z.P., 2017. Size effect on punching strength of reinforced concrete slabs with and without shear reinforcement. ACI Struct. J. 114 (4), 875.
Dönmez, A., Bažant, Z.P., 2019. Critique of critical shear crack theory for fib model code articles on shear strength and size effect of reinforced concrete beams. Struct. Concr. 20 (4), 1451–1463.
Duckett, W., 2005. Risk analysis and the acceptable probability of failure. Struct. Eng. 83 (15).
Dutta, A., Tekalur, S.A., 2014. Crack tortuousity in the nacreous layer–topological dependence and biomimetic design guideline. Int. J. Solids Struct. 51 (2), 325–335.
Dutta, A., Tekalur, S.A., Miklavcic, M., 2013. Optimal overlap length in staggered architecture composites under dynamic loading conditions. J. Mech. Phys. Solids 61 (1), 145–160.
Evans, A., 1972. A method for evaluating the time-dependent failure characteristics of brittle materials—and its application to polycrystalline alumina. J. Mater. Sci. 7 (10), 1137–1146.
Evans, A., Fu, Y., 1984. The mechanical behavior of alumina. Fract. Ceramic Mater. 56–88.
Fett, T., 1992. A fracture-mechanical theory of subcritical crack growth in ceramics. Int. J. Fract. 54 (2), 117–130.
Fett, T., Munz, D., 1990. Static and cyclic fatigue of ceramic materials. In: Ceramics Today- Tomorrow's Ceramics. Proc. 7 Th Int. Meeting on Modern Ceramics Technologies(7 Th CIMTEC- World Ceramics Congress). Part C Montecatini Terme, 24-30 June 1990. pp. 1827–1835.
Fisher, R.A., Tippett, L.H.C., 1928. Limiting forms of the frequency distribution of the largest or smallest member of a sample. Math. Proc. Camb. Phil. Soc. 24 (2), 180–190.
Gao, H., Ji, B., Jäger, I.L., Arzt, E., Fratzl, P., 2003. Materials become insensitive to flaws at nanoscale: lessons from nature. Proc. Natl. Acad. Sci. 100 (10), 5597–5600.
Glasstone, S., Laidler, K., Eyring, H., 1941. Theory of Rate Processes. Vol. 20, McGraw-Hill, New York.
Graham-Brady, L., Arwade, S., Corr, D., Gutierrez, M., Breysse, D., Grigoriu, M., Zabaras, N., 2006. Probability and materials: from nano-to macro-scale: A summary. Probab. Eng. Mech. 21 (3), 193–199.
Griffith, A.A., 1921. VI. The phenomena of rupture and flow in solids. Philos. Trans. R. Soc. Lond. Ser. A 221 (582–593), 163–198.
Gumbel, E.J., 2004. Statistics of Extremes. Courier Corporation.
Haldar, A., Mahadevan, S., 2000. Probability, Reliability, and Statistical Methods in Engineering Design. John Wiley & Sons Incorporated.
Harlow, D.G., Phoenix, S.L., 1978. The chain-of-bundles probability model for the strength of fibrous materials I: Analysis and conjectures. J. Compos. Mater. 12 (2), 195–214.
Harlow, D.G., Phoenix, S.L., 1979. Bounds on the probability of failure of composite materials. Int. J. Fract. 15 (4), 321–336.
Harlow, D., Smith, R., Taylor, H., 1983. Lower tail analysis of the distribution of the strength of load-sharing systems. J. Appl. Probab. 20 (2), 358–367.
Hubler, M.H., Wendner, R., Bažant, Z.P., 2015. Statistical justification of model B4 for drying and autogenous shrinkage of concrete and comparisons to other models. Mater. Struct. 48 (4), 797–814.
Hutchinson, J., 1968. Singular behaviour at the end of a tensile crack in a hardening material. J. Mech. Phys. Solids 16 (1), 13–31. http://dx.doi.org/10.1016/0022-5096(68)90014-8.
Ibnabdeljalil, M., Phoenix, S.L., 1995. Creep rupture of brittle matrix composites reinforced with time dependent fibers: Scalings and Monte Carlo simulations. J. Mech. Phys. Solids 43 (6), 897–931.
Iguro, M., Shioya, T., Nojiri, Y., Akiyama, H., 1984. Experimental studies on the shear strength of large reinforced concrete beams under uniformly distributed load. Doboku Gakkai Ronbunshu 1984 (348), 175–184.
Irwin, G.R., 1958. Fracture. Handbuch Der Physik 6, 551.
Jayatilaka, A.d.S., Trustrum, K., 1977. Statistical approach to brittle fracture. J. Mater. Sci. 12 (7), 1426–1430.
Kramers, H.A., 1940. Brownian motion in a field of force and the diffusion model of chemical reactions. Physica 7 (4), 284–304.
Krausz, A.S., 1988. Fracture Kinetics of Crack Growth. Vol. 1, Springer Science & Business Media.
Le, J.-L., 2015. Size effect on reliability indices and safety factors of quasibrittle structures. Struct. Saf. 52, 20–28.
Le, J.-L., Ballarini, R., Zhu, Z., 2015. Modeling of probabilistic failure of polycrystalline silicon MEMS structures. J. Am. Ceram. Soc. 98 (6), 1685–1697.
Le, J.-L., Bažant, Z.P., 2012. Scaling of static fracture of quasi-brittle structures: strength, lifetime, and fracture kinetics. J. Appl. Mech. 79 (3).
Le, J.-L., Bažant, Z.P., Bazant, M.Z., 2011. Unified nano-mechanics based probabilistic theory of quasibrittle and brittle structures: I. Strength, static crack growth, lifetime and scaling. J. Mech. Phys. Solids 59 (7), 1291–1321.
Le, J.-L., Manning, J., Labuz, J.F., 2014. Scaling of fatigue crack growth in rock. Int. J. Rock Mech. Min. Sci. 72, 71–79.
Le Chatelier, H., 1887. Recherches Expérimentales sur la Constitution Des Ciments Hydrauliques. Imprimerie C. Marpon et E. Flammarion.
Lohbauer, U., Petschelt, A., Greil, P., 2002. Lifetime prediction of CAD/CAM dental ceramics. J. Biomed. Mater. Res.: Off. J. Soc. Biomater., Japanese Soc. Biomater., Australian Soc. Biomater. Korean Soc. Biomater. 63 (6), 780–785.

Luo, W., Bažant, Z.P., 2017. Fishnet statistics for probabilistic strength and scaling of nacreous imbricated lamellar materials. J. Mech. Phys. Solids 109, 264–287.
Luo, W., Bažant, Z.P., 2018. Fishnet model with order statistics for tail probability of failure of nacreous biomimetic materials with softening interlaminar links. J. Mech. Phys. Solids 121, 281–295.
Luo, W., Bažant, Z.P., 2020. General fishnet statistics of strength: Nacreous, biomimetic, concrete, octet-truss, and other architected or quasibrittle materials. J. Appl. Mech. 87 (3).
Mahesh, S., Phoenix, S., 2004. Lifetime distributions for unidirectional fibrous composites under creep-rupture loading. Int. J. Fract. 127 (4), 303–360.
Mazars, J., 1981. Mechanical damage and fracture of concrete structures. Adv. Fracture Res. 4, 1499–1506.
Melchers, R.E., Beck, A.T., 2018. Structural Reliability Analysis and Prediction. John Wiley and sons.
Munz, D., Fett, T., 1999. Ceramics: Mechanical Properties, Failure Behaviour, Materials Selection. Vol. 36, Springer Science and Business Media.
Nguyen, H.T., Caner, F.C., Bažant, Z.P., 2021a. Conversion of explicit microplane model with boundaries to a constitutive subroutine for implicit finite element programs. Internat. J. Numer. Methods Engrg. 122 (6), 1563–1577.
Nguyen, H.T., Dönmez, A.A., Bažant, Z.P., 2021b. Structural strength scaling law for fracture of plastic-hardening metals and testing of fracture properties. Extreme Mech. Lett. 43, 101141.
Nguyen, H., Pathirage, M., Cusatis, G., Bažant, Z.P., 2020a. Gap test of crack-parallel stress effect on quasibrittle fracture and its consequences. J. Appl. Mech. 87 (7).
Nguyen, H., Pathirage, M., Rezaei, M., Issa, M., Cusatis, G., Bažant, Z.P., 2020b. New perspective of fracture mechanics inspired by gap test with crack-parallel compression. Proc. Natl. Acad. Sci. 117 (25), 14015–14020.
Nguyen, H.T., Rahimi-Aghdam, S., Bažant, Z.P., 2019. Sorption isotherm restricted by multilayer hindered adsorption and its relation to nanopore size distribution. J. Mech. Phys. Solids 127, 111–124.
Nguyen, H., Rahimi-Aghdam, S., Bažant, Z.P., 2020. Unsaturated nanoporomechanics. Proc. Natl. Acad. Sci. 117 (7), 3440–3445.
Nitka, M., Tejchman, J., 2015. Modelling of concrete behaviour in uniaxial compression and tension with dem. Granular Matter 17 (1), 145–164.
Okamura, H., Higai, T., 1980. Proposed design equation for shear strength of reinforced concrete beams without web reinforcement. Proc. Japan Soc. Civ. Eng. 1980 (300), 131–141.
Phillips, R., Rob, P., 2001. Crystals, Defects and Microstructures: Modeling Across Scales. Cambridge University Press.
Phoenix, S.L., 1978a. The asymptotic time to failure of a mechanical system of parallel members. SIAM J. Appl. Math. 34 (2), 227–246.
Phoenix, S.L., 1978b. Stochastic strength and fatigue of fiber bundles. Int. J. Fract. 14 (3), 327–344.
Phoenix, S., Ibnabdeljalil, M., Hui, C.-Y., 1997. Size effects in the distribution for strength of brittle matrix fibrous composites. Int. J. Solids Struct. 34 (5), 545–568.
Phoenix, S.L., Tierney, L., 1983. A statistical model for the time dependent failure of unidirectional composite materials under local elastic load-sharing among fibers. Eng. Fract. Mech. 18 (1), 193–215.
Reineck, K.-H., Kuchma, D.A., Kim, K.S., Marx, S., 2003. Shear database for reinforced concrete members without shear reinforcement. ACI Struct. J. 100 (2), 240–249.
Rice, J.R., 1968. A path independent integral and the approximate analysis of strain concentration by notches and cracks. J. Appl. Mech. 35 (2), 379–386. http://dx.doi.org/10.1115/1.3601206.
Rice, J., Rosengren, G., 1968. Plane strain deformation near a crack tip in a power-law hardening material. J. Mech. Phys. Solids 16 (1), 1–12. http://dx.doi.org/10.1016/0022-5096(68)90013-6.
Rice, J.R., et al., 1968. Mathematical analysis in the mechanics of fracture. Fracture: Adv. Treatise 2, 191–311.
Rosen, B.W., 1964. Tensile failure of fibrous composites. AIAA J. 2 (11), 1985–1991.
Shao, Y., Zhao, H.-P., Feng, X.-Q., Gao, H., 2012. Discontinuous crack-bridging model for fracture toughness analysis of nacre. J. Mech. Phys. Solids 60 (8), 1400–1419.
Smith, R.L., 1982. The asymptotic distribution of the strength of a series-parallel system with equal load-sharing. Ann. Probab. 137–171.
Syroka-Korol, E., Tejchman, J., 2014. Experimental investigations of size effect in reinforced concrete beams failing by shear. Eng. Struct. 58, 63–78.
Thouless, M., Hsueh, C., Evans, A., 1983. A damage model of creep crack growth in polycrystals. Acta Metall. 31 (10), 1675–1687.
Tobolsky, A., Eyring, H., 1943. Mechanical properties of polymeric materials. J. Chem. Phys. 11 (3), 125–134.
Wagner, H., 1989. Stochastic concepts in the study of size effects in the mechanical strength of highly oriented polymeric materials. J. Polym. Sci. B: Polym. Phys. 27 (1), 115–149.
Wang, R., Suo, Z., Evans, A., Yao, N., Aksay, I.A., 2001. Deformation mechanisms in nacre. J. Mater. Res. 16 (9), 2485–2493.
Wei, X., Filleter, T., Espinosa, H.D., 2015. Statistical shear lag model–unraveling the size effect in hierarchical composites. Acta Biomater. 18, 206–212.
Weibull, W., 1939. The phenomenon of rupture in solids. Proc. Royal Swedish Inst. Engrg. Res. 153, 1–55.
Wendner, R., Hubler, M., Bažant, Z., 2013. The B4 model for multi-decade creep and shrinkage prediction. In: 9th International Conference on Creep, Shrinkage, and Durability Mechanics: A Tribute To Zdeněk P. Bažant, CONCREEP 2013. American Society of Civil Engineers (ASCE), pp. 429–436.
Xu, Z., Le, J.-L., 2018. On power-law tail distribution of strength statistics of brittle and quasibrittle structures. Eng. Fract. Mech. 197, 80–91.
Yu, Q., Le, J.-L., Hubler, M.H., Wendner, R., Cusatis, G., Bažant, Z.P., 2016. Comparison of main models for size effect on shear strength of reinforced and prestressed concrete beams. Struct. Concr. 17 (5), 778–789.
Zhang, X., Vyatskikh, A., Gao, H., Greer, J.R., Li, X., 2019. Lightweight, flaw-tolerant, and ultrastrong nanoarchitected carbon. Proc. Natl. Acad. Sci. 116 (14), 6665–6672.
Zhurkov, S., Korsukov, V., 1974. Atomic mechanism of fracture of solid polymers. J. Polym. Sci.: Polym. Phys. Edition 12 (2), 385–398.